The Derivation of a Sub-Canopy Digital Terrain Model of a Flooded Forest Using Synthetic Aperture Radar

Marc Lee Imhoff
NASA/Goddard Space Flight Center, Greenbelt, MD 20771
Dean B. Gesch
ST Systems Corporation (STX), Lanham, MD 20706

ABSTRACT: Synthetic aperture radar data from the Shuttle Imaging Radar-B Mission were combined with tide surface information to create a digital terrain model for a 70-km by 40-km section of the Mouths of the Ganges forests in southern Bangladesh. The dominance of the interaction phenomenon (canopy to surface or surface to canopy reflection) in flooded forests was exploited to create sub-canopy flood boundary maps for two different tide times. The boundary maps were digitally combined in x,y,z space with tide elevation models created from tide gauge data gridding the survey site and used as input to interpolation routines to create a terrain model. The end product represents a significant step in our ability to characterize the topography and hydrology of wetland ecosystems. The model derived here can be used for simulating tidal flow and nutrient transport from the forest to the marine habitat.

INTRODUCTION

MANGROVES OR WET COASTAL FOREST ECOSYSTEMS are an important resource throughout the tropic and subtropic regions of the globe. As a whole, mangrove formations account for a significant share of the forested coastlines of these regions (Chapman, 1975) and are an important source of biological productivity. By providing environments for abundant plant, algal, and marine and terrestrial animal life, mangroves figure prominently in the cycling of organic matter (Golly *et al.*, 1962) and may be more fertile than many marine and terrestrial communities.

A critical environmental factor in the formation and health of a mangrove ecosystem is the surface hydrology. Lugo and Snedaker (1974) listed the two most important factors as tidal dynamics and water chemistry. Both of these factors are critically interactive with the geomorphology or substrate topography upon which the mangroves evolve. The topographic contour of a mangrove formation substrate will determine the frequency of the flooding and the chemistry of the flood waters and thus the productivity and health of the stand.

Synthetic aperture radar data can be used to help provide this sort of information. Radar imagery has been used to delineate flooded surfaces beneath forest canopies in diverse situations. Waite and MacDonald (1971) first noted that flooded forests in "leaf off" conditions in Arkansas showed up as anomalously bright areas on K-band radar images. MacDonald *et al.* (1980) and Waite *et al.* (1981) observed this to be a "penetration" phenomenon in similar circumstances using L-band SEASAT data. Other scientists (Krohn *et al.*, 1983; Ormsby *et al.*, 1985; Hoffer *et al.*, 1986) have also noted it in L-band radar imagery acquired at different angles of incidence in fully leafed forest conditions in eastern Maryland, Virginia, and Florida, respectively.

OBJECTIVE

The objective of this study was to explore the use of radar imagery for deriving topographic information in mangrove formations by coupling radar derived inundation parameters with tide surface elevation models developed from data acquired in the field.

STUDY AREA AND DATA ACQUISITION

THE SURVEY AREA

The study area is a 70-km by 40-km section of a tide-river dominated allochthonous mangrove formation at the Mouths of the Ganges river in southern Bangladesh (Figures 1a,1b, and 1c). This formation is locally known as the Sundarbans Forest and forms the northern boundary of the Bay of Bengal. The forest was surveyed and mapped into classes by the British Overseas Development Administration (BODA) for Bangladesh in 1984 using aerial photography (BODA, 1985). The forest is populated primarily by two mangrove tree species: Sundri (*Heritiera minor* Syn. *H. fomes*) and Gewa (*Excoecaria agallocha*). The predominant forest classes in the area are combinations of Sundri and Gewa classified as percentages of the two species, average height of the stand, and canopy closure. The predominant forest classes in the area are shown in Figure 4a. Canopy or crown closures in the forest as whole range between 100 percent and 30 percent with the most common closure class being 75 to 100 percent closed. An average tree height of 12.5 metres prevails for both species. A primary characteristic of the Sundri trees is their production of vertical root structures called pneumatophores. These structures, which may provide a means for the species to acquire oxygen during high tides, vary in height from a few centimetres to almost two metres, and can be found in large numbers in some stands.

The forest floor is devoid of rock outcrops, consists of a silty clay loam, and has a range in elevation of about 3 metres. In this instance, the higher ground is found near the stream edges and the lower ground near the center of the islands. This trend in shape is a result of a tendency for the drainage channels to aggrade, thus eventually forming a concave shape to the geomorphically older portions of the formation (Deb, 1956).

RADAR DATA

The radar data used to create the model consisted of three digital HH polarized L-band (23.5-cm wavelength or approximately 1GHz) radar images acquired at 26°, 46°, and 58° angles of incidence. The data were collected as part of the Shuttle Imaging Radar B (SIR-B) mission (Cimino *et al.*, 1986) in October 1984 (Table 1 and Figure 2). All three data sets were four-look processed, registered in ground range, and resampled to 25-m^2

PHOTOGRAMMETRIC ENGINEERING AND REMOTE SENSING,
Vol. 56, No. 8, August 1990, pp. 1155–1162

0099-1112/90/5608–1155$02.25/0

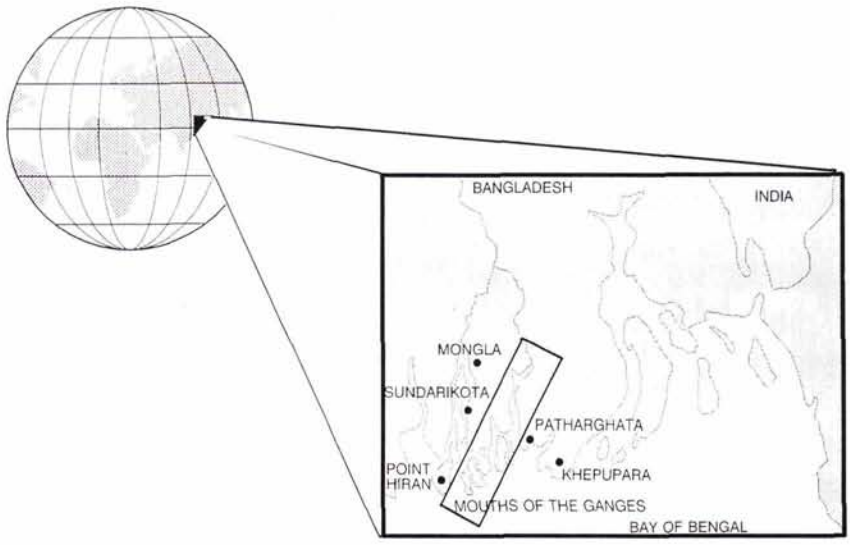

(a)

(b)

(c)

FIG. 1. (a) Location of the experiment site and tide gauge stations. (b) Aerial view of a portion of the study area taken during the dry season. (c) A view of forest floor in a stand of lesser density (30 percent closed). Note pneumatophores and partial flooding. Water level can vary from a few inches to a few metres.

pixels for registration purposes. The original cell sizes are shown in Table 1.

FIELD DATA

Reference data used in this study consisted of 1:30,000-scale black-and-white and color infrared aerial photography (acquired in the dry season), 1:30,000-scale Forest Survey Maps, tide gauge data from five stations distributed throughout a region slightly larger than the survey area, a 1200-m topographic survey transect, and numerous test plots in the forest which were visited during the data acquisition period. The BODA used the aerial photography to map canopy closures and verify tree heights and stand classification.

Tide elevation readings from five stations (shown in Figure 1a.) were used to define tide surfaces spanning the survey area. The tide elevation data are relative to mean sea level (MSL) and were taken during radar data acquisition as well as during the topographic profile survey. Tide surface elevation models corresponding to four instants in time (three radar data acquisitions plus the time of the survey transect) were generated using a first-order polynomial interpolation. Once generated, the tide elevation models were stored as images and were geometrically registered to the radar imagery.

TABLE 1. SIR - B RADAR ACQUISITION OVER BANGLADESH

Data Take (DT)	Date Acquired	Time GMT	Time Local*	Incidence Angle	Bits/ Sample	Ground Resolution (m) Range	Ground Resolution (m) Azimuth
88	10 Oct 84	284/21:05:51	3:06AM	57.8°	5	16.6	31.1
104	11 Oct 84	285/20:48:21	2:48AM	45.6°	5	19.8	33.7
120	12 Oct 84	286/20:30:41	2:30AM	25.8°	4	32.2	28.3

*Local dates are 11 Oct 84, 12 Oct 84, and 13 Oct 84.

A topographic transect or profile was acquired using standard leveling techniques. Elevation measures were made every 30 metres for a distance of 1200 m across one of the islands in the survey region. The elevation measures acquired in the survey were tied to the water level existing in the main channel so that the land elevations were assigned values relative to the tide

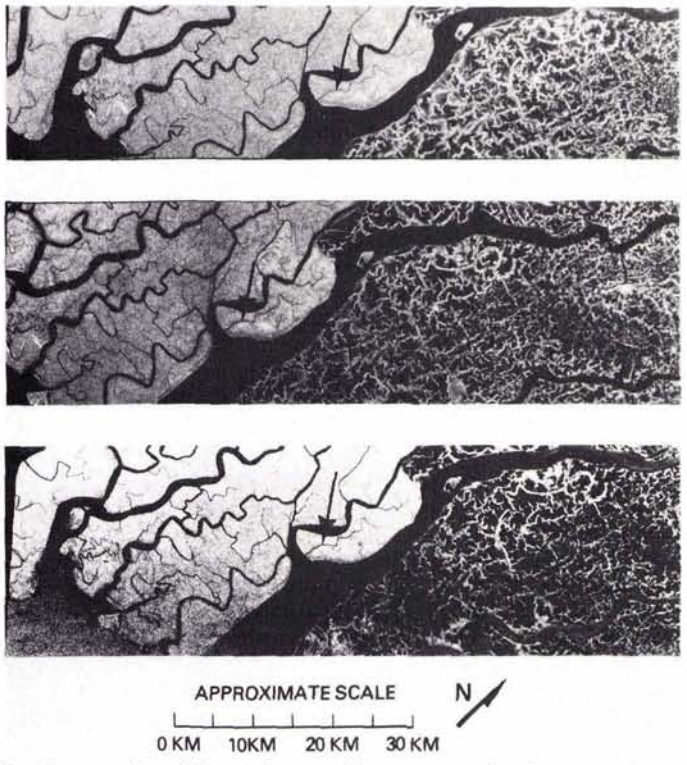

FIG. 2. SIR-B data of the study area. Three successive data acquisitions are shown. From top are Data Take (DT) 88 ($\theta i = 58°$), DT 104 ($\theta i = 46°$), and DT 120 ($\theta i = 26°$). Location of the 1200-metre survey transect is marked by an arrow.

surface model matching that point in space and time (Figure 3). Originally, only one part of the mangrove formation was targeted for study so only one transect was taken. Ideally, many transects should be made although surveying in these environments is very difficult and expensive. Techniques used to expand the test area are described in the next section.

RESULTS AND DISCUSSION

Data Analysis

The radar data, the field data consisting of the transect profile and site observations, and the tide elevation models were all digitally co-registered for analysis. The co-registration, data processing, and analysis were carried out using the Land Analysis System (LAS) software at NASA/Goddard Space Flight Center's Image Analysis Facility (IAF).

The radar data for each pass were calibrated using Active Radar Calibrators and passive corner reflectors located in the test site during the shuttle data acquisition. The transfer functions for converting the bit image values to values representing a radar backscattering coefficient σ^o in dB (m^2/m^2) were derived using a technique described by Dobson *et al.* (1986). Although applied here, the rendering of radar image digital numbers (DN) to dB was not required for model development.

Flood Boundary Delineation

Mean radar response values for flooded and non-flooded forest areas were calculated from training sets distributed throughout the region. Training site selection was based on the following criteria: (1) The region's major forest cover classes should be represented, (2) the samples must be distributed so that there is topographic variability among samples, and (3) the condition of the Surface Boundary Layer (SBL) as flooded or non-flooded should be known for each site. These criteria were met for a limited number of sites near the survey transect and by point verification by site visits for others. Sample plots were located representing four predominant forest classes. Two plots for each class were located where one plot was located on high ground and another on low ground. Each plot averaged over 100 samples for a total of 502 samples on high ground and 606 samples on the lower ground.

Mean response values, both in the form of DN and their corresponding σ^o values, were generated for the designated sample sites (Figure 4a). Comparisons were then made between the radar response values for the training sets for each of the three radar incidence angles. A plotting of the backscatter coefficients showed that the radar response for identical forest classes varied considerably, but consistently, forming two clusters at higher and lower intensities. It appeared that sites located at different points along the transect varied significantly depending upon their topographic position relative to the tide surfaces. Forest areas that were located topographically inferior to the tide surfaces all had statistically higher mean radar backscatter than those test plots that were superior in elevation. This was taken as evidence that flooded forest stands exhibited distinctly higher response values as verified by the survey transect. Once SBL conditions were verified, the test sites were separated into flooded and non-flooded categories and new statistics generated (Figure 4b).

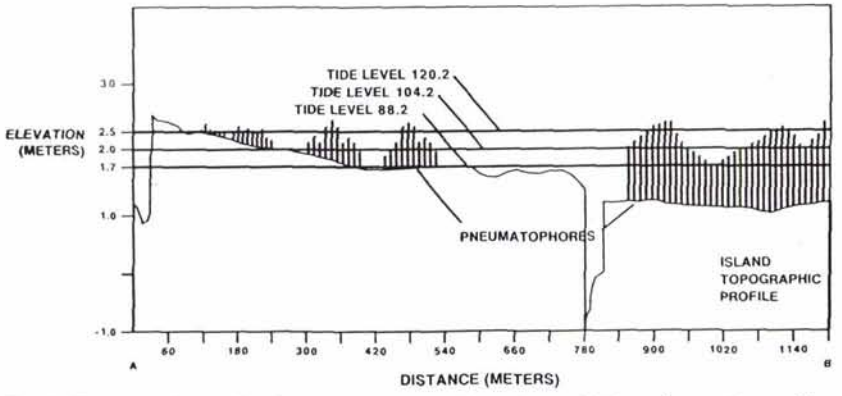

FIG. 3. Topographic profile of survey transect with registered tide surfaces shown. The transect data were used to help define training sets for analyzing the backscatter of flooded versus non-flooded conditions. The tide levels are referenced by the SIR-B Data Take (DT) number which was acquired at that tide time.

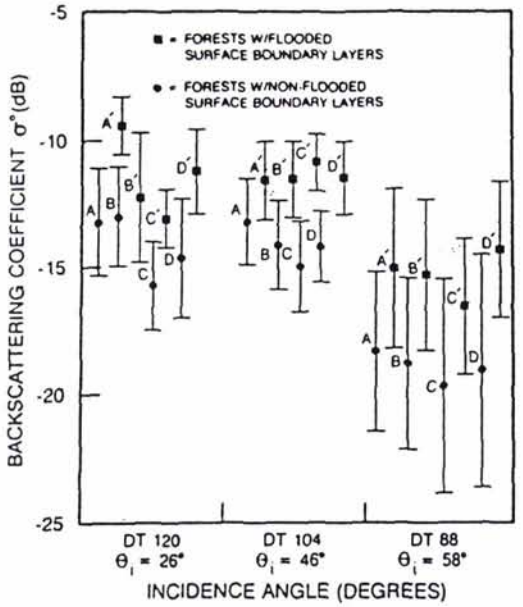

KEY

SYMBOL	FOREST TYPE	CANOPY CLOSURE	HEIGHT CLASS (M)
A	SUNDRI-GEWA	75%-100%	<15 ≥10
B	GEWA-SUNDRI	75%-100%	<15 ≥10
C	GEWA-SUNDRI	75%-100%	<10 ≥5
D	GEWA	75%-100%	<15 ≥10
(′) PRIME	DENOTES FLOODED SURFACE BOUNDARY LAYER CONDITION		

(a)

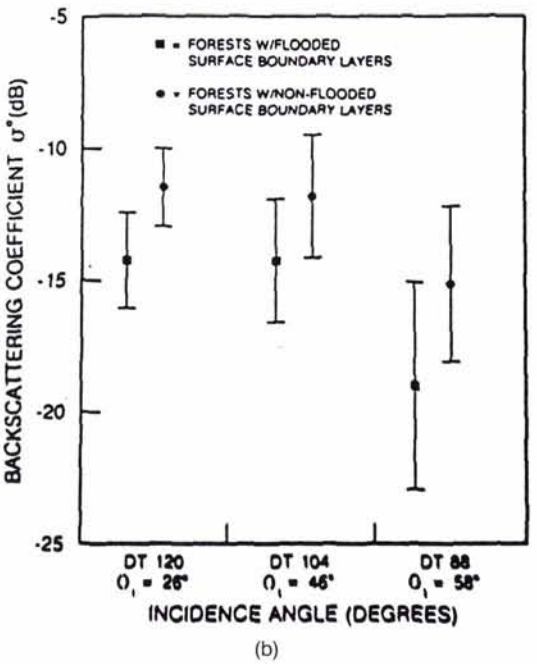

(b)

FIG. 4. (a) Backscatter plot with mean and standard deviation of four forest classes with flooded and non-flooded conditions for all three data takes. Only forest classes with >75 percent closed canopies were used. (b) Plot of group statistics showing mean backscatter of flooded and non-flooded conditions for all forests. The results of a Z-test indicated that a significant difference exists between them at the $\alpha = 0.01$ level of confidence.

A Z test was performed to provide a measure of separability on the new means. The test was designed as follows:

$$\text{HO: } \mu \text{ dry} = \mu \text{ wet}$$

$$Z = \frac{X \text{ dry} - X \text{ wet}}{\sqrt{\frac{\sigma^2 \text{ dry}}{n \text{ dry}} + \frac{\sigma^2 \text{ wet}}{n \text{ wet}}}}$$

The test was performed for each data take using an $\alpha = 0.01$ level of confidence. The results of this test showed a significant difference between categories for all data takes, indicating that the radar could be used to delineate flooded forest boundaries with a reasonable degree of confidence.

The difference in reflectivity between flooded and non-flooded forests is apparently due to the substantial differences in the SBL. The presence of a smooth reflective surface boundary layer, as would be present in a flooded forest, creates a multiple corner reflector effect between the tree stands and the SBL. Radar radiation reflects off the smooth SBL and onto the tree trunks (or vice versa) and then up into the canopy and back toward the radar, creating a response which is brighter than a non-flooded forest (Imhoff *et al.*, 1986). This mechanism has been modeled mathematically by Enghata and Elachi (1984), Richards *et al.* (1986), and Ulaby *et al.* (1986). This canopy-to-surface or surface-to-canopy backscatter mechanism has been called the interaction phenomenon or a two-bounce return (i.e., specular plus corner reflector). In canopies of lesser density, this effect can become dominant especially at the longer wavelengths. At shorter wavelengths, canopy scattering may dominate. Canopy dominance in the backscatter would make SBL contributions (if any) imperceptible, thereby preventing flood boundary delineation. Discussion of this effect with respect to radar polarization can be found in a work by Zebker *et al.* (1987).

Inundation Mapping

The DN counterparts to the mean backscatter coefficients derived from the test sites were used to select break points for classifying the radar imagery into flooded versus non-flooded forests. The radar imagery acquired at the 58° and 46° angles (DT 88 and DT 104) were filtered serially through one iteration using first a 5 by 5 and then an 11 by 11 median filter. The spatial filtering served to eliminate image speckle and created an image texture more suitable for generating discrete classes at a spatial frequency appropriate to the formation. The basis for using such spatial filtering techniques for SAR data can be found in a work by Daily (1983).

The generation of discrete classes was accomplished by means of density slicing controlled by the mean DN level values as breakpoints. The density sliced image for each data pass represented a flood boundary map effective for that tide stage. The two images were merged by means of bit mask addition to produce a combined inundation map showing three inundation classes; two classes of successive inundation (taken from the 58° and 46° incident angle data) and a third class representing all areas not flooded during either of the two tide times (Figure 5). An additional class of successive inundation could have been generated using the 26° incident angle data (DT 120) which was collected at the highest tide level coinciding with the radar data. Early on in the project, however, there was some uncertainty in the tide gauge measurement assigned for that date. By the time the tide measures were verified for the 26° data, the model was in an advanced stage of development so the inundation information was not used. The 26° data was used, however, to verify the Land Edge Boundary, which was never in question. The tide level present for the 26° data is correctly shown in Figure 3.

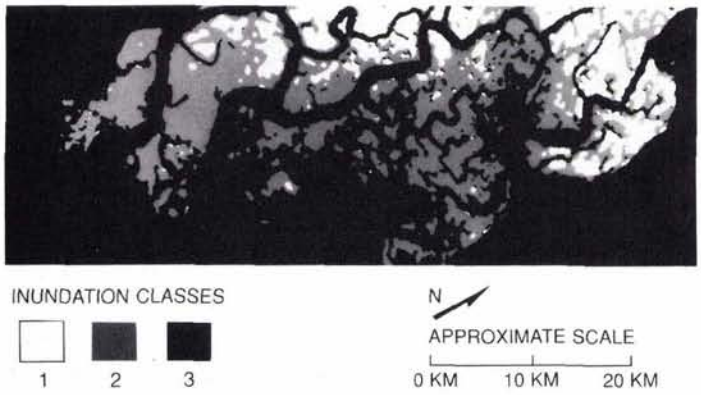

FIG. 5. Density sliced merged radar image showing three categories of inundation.

TOPOGRAPHIC MODEL GENERATION

The inundation class map was turned into a topographic product by matching the appropriate class boundaries to the tide elevation models. This was done in the image domain by bit masking the flood boundaries into separate entitites and multiplying each boundary set by the appropriate tide elevation image (Figures 6 and 7).

The high end boundary for the never-flooded class was quantified to elevation values by matching it to a surface generated from a single measurement (made at the survey transect) extended spatially by a heuristic based on observations. This was done mainly due to a lack of survey data. The heuristic simply states that the maximum land elevation in the entire region is never more than 2 metres above the tide surface elevation. This was found to be generally true from observations made at various locations in the region during the time the topographic transect survey was made. The heuristic was used to form a Maximum Land Elevation surface to close the model.

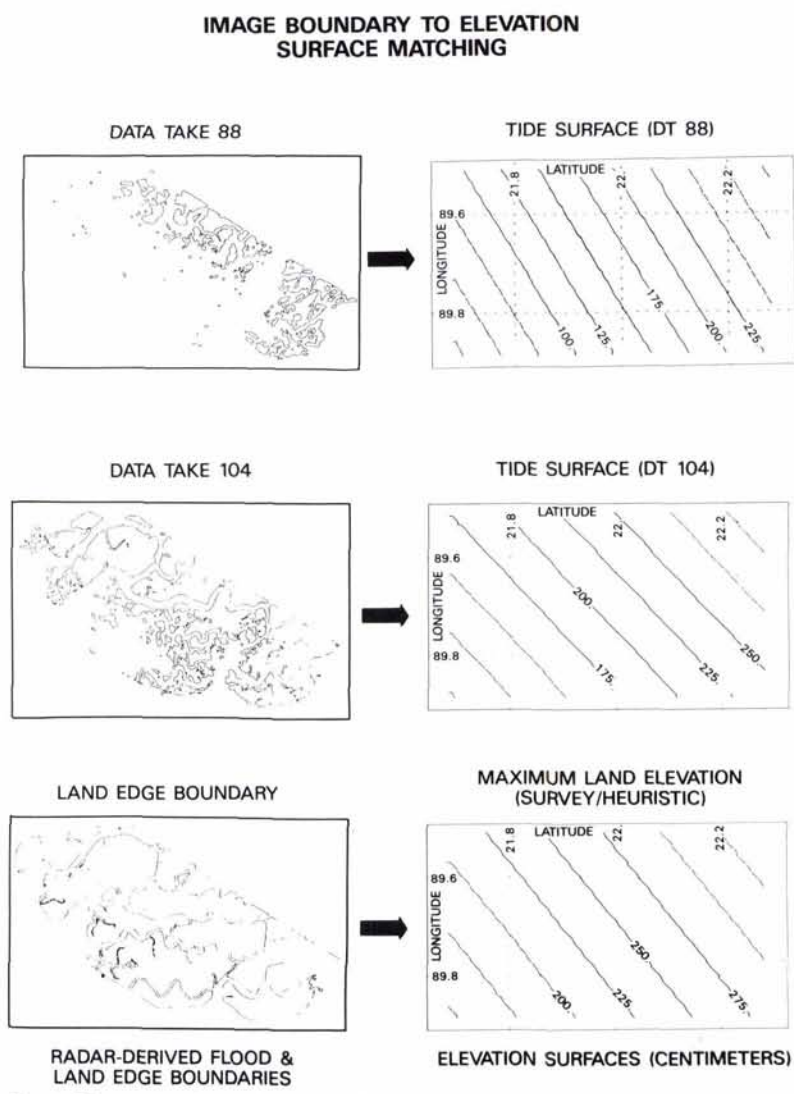

FIG. 6. Figure showing radar derived flood boundaries stripped off each imaged for merger with the appropriate tide surface elevation model. Data take 120 was used to create the Land Edge Boundary. All images and tide surface models are co-registered. From Top: Data Take (DT) 88 ($\theta i = 58°$), DT 104 ($\theta i = 46°$), and DT 120 ($\theta i = 26°$).

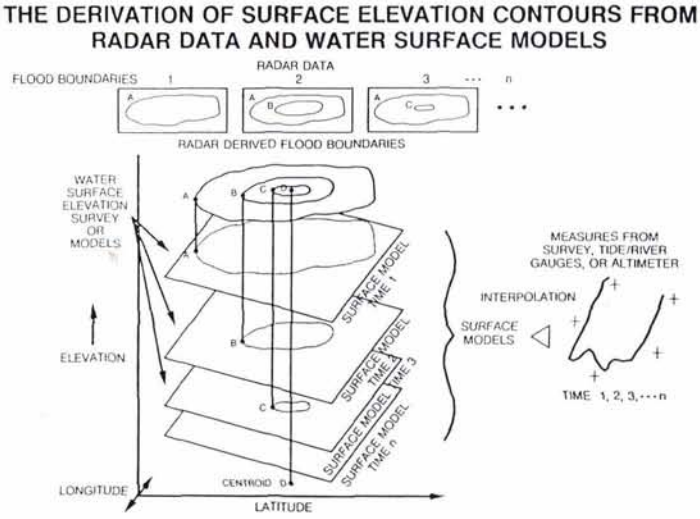

FIG. 7. Graphic outline of methodology for incorporating radar derived flood boundaries and tide surface data into a digital terrain model.

The heuristic was necessary to provide a bound to an otherwise open-ended model.

The merger of each boundary set to its appropriate tide surface elevation surface model resulted in new image products where each pixel in a boundary now had as its value a real elevation number referencable to MSL. These products were then recombined to form an image of elevation values in place of the simple inundation boundaries. The elevation product was subsampled in order to reduce the data to a distributed set of control points for interpolation. An interpolation routine was used to create the digital terrain model (DTM). The interpolation techniques used to generate both the tide surfaces and the land elevation models were implemented using the LAS program SURFACE. The SURFACE program simultaneously weights the control point values using an inverse distance relation and the direction of the points from a local origin (Shepherd, 1968). Several search functions can be used depending upon the distribution of the control points. For the tide surface data, where the control points were widely distributed, a simple trend surface was generated by a least-squares fitting of a two-dimensional polynomial. For the land elevation data, however, an octant search was used. Because the elevation control points for the land surface were defined from the contour following flood boundaries, they tended to be aggregated into strings. The octant search option was better suited for dealing with this sort of distribution.

Views of the Model

The interpolation of the land elevation data resulted in a digital terrain model of the entire 40-km by 70-km segment of the island formation. Different views of the radar-derived DTM were generated using the National Space Science Data Center's Graphics System (NGS) at GSFC (Treinish, 1986). Topographic contour maps, flat elevation class images, and perspective view products allowed for a first-ever view of the sub-canopy topography of the forest (Figures 8 and 9 and Plate 1). Internal calculations can be made to estimate tide volumes and flow rate given a particular tide scenario.

ERROR

The topographic product described here is generally true according to what is known about the Mouths of the Ganges forests; however, like any model, there are some inherent inaccuracies. Some of these inaccuracies are due to interpolation error and resolution which are common to all models, while others relate directly to the SAR technique or simple deficiencies in the data sets.

Error Due to Lack of Data

A lack of elevation tie point data and radar imagery represent sources of error which affect this model. Additional survey tie points would stabilize the model spatially by eliminating the

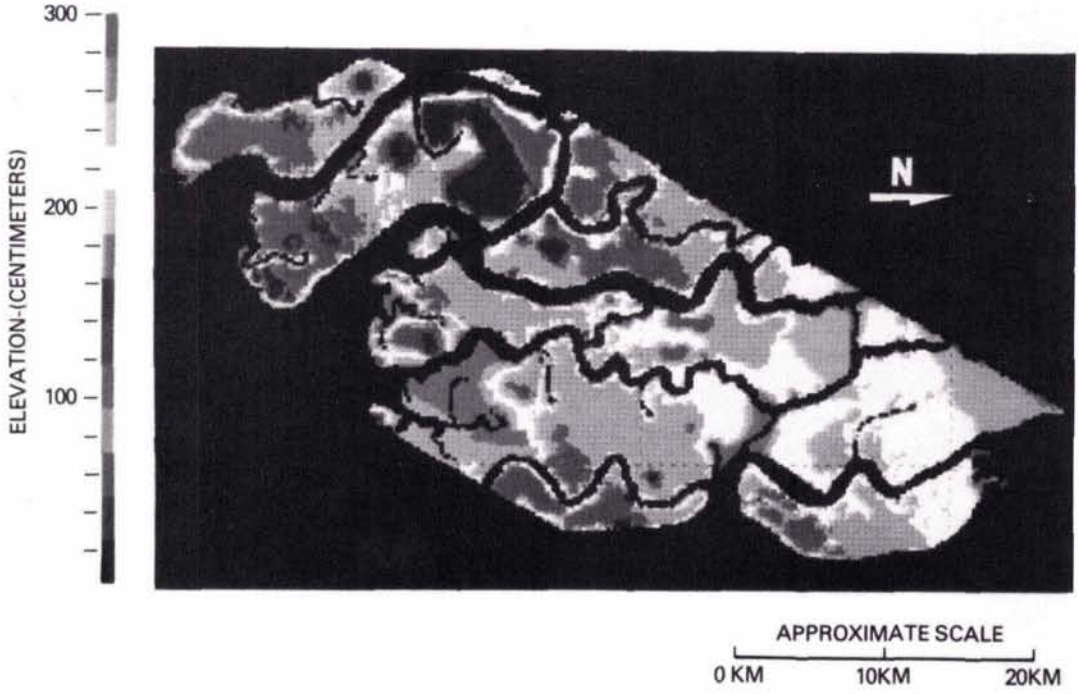

FIG. 8. A two-dimensional color coded contour class map of the entire 40- by 70-km formation. Elevations are in 5-cm classes.

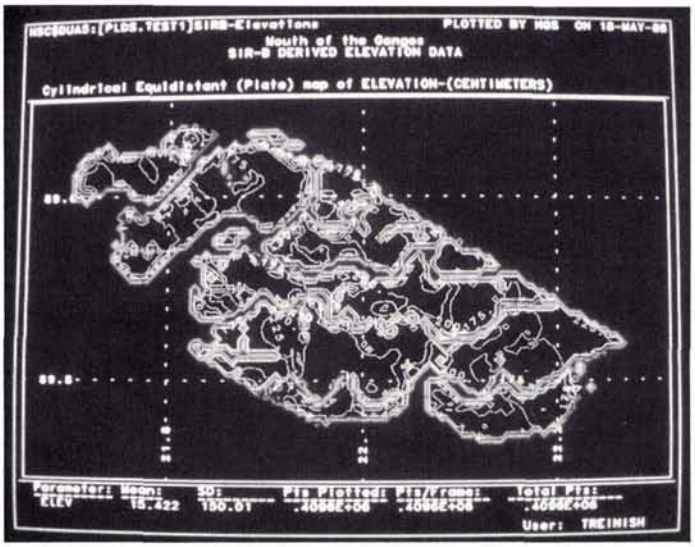

FIG. 9. A standard contour line type product of the formation. Contour line scaling was determined by the graphics package and is at 10-cm intervals.

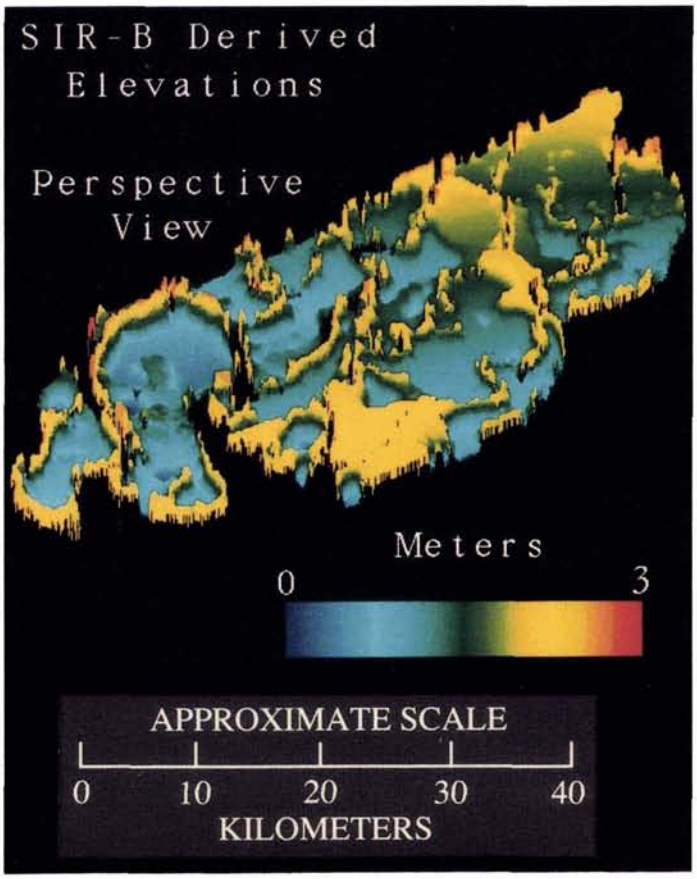

PLATE 1. Perspective view of digital terrain model.

need to use a heuristic too create the Maximum Land Elevation Surface as an extension from a single tie point. Additional tie points would permit the generation of a more accurate and spatially stable surface model for application to the upper land surface boundary. Stability in the model derived here is totally dependent upon the truth-in-extendibility of the heuristic which is only qualitatively known. Measurement error, or lack of precision, can also be introduced to the model as a result of the tide elevation surfaces because they were used to reference the land surface elevations. If only a few data points are available for interpolation, as was true in this case, then a low order polynomial must be used, making the model coarse. Outright errors in tide gauge measurement will certainly induce errors into the whole model. In addition, a tide-surface-related error will result from lag times associated with interior drainage of the formation. Because this occurs at a scale that is relatively large, however, this error can be considered inconsequential when creating a small scale large area model.

The model presented here is also somewhat coarse in topographic resolution or "fit" due to a lack of radar data. More radar images taken at successional stages of inundation would fill in the contour resolution internally as well as reduce the surface area affected by the application of the upper and lower bounding limits. Additional radar data at higher and lower tide levels, for example, would have closed the upper and lower ends of the terrain model with final elevation classes substantially smaller in area than those resulting here. This would have served to "round out" the otherwise topographically flat nature of the upper and lower elevation bounding classes. The improvement of accuracy through the addition of data would have to be traded off against the corresponding increase in the cost of generating the model.

Error Related to the Delineation of Flood Boundaries

Although a statistically significant separation could be made between flooded versus non-flooded forest areas using the test sites in this study, variations in canopy structure, density, and the radar incidence angle could make accurate separation difficult or even impossible in some instances (see Imhoff *et al.*, 1986). Even though some field checking was done and the resulting topographic model matches the known geomorphology quite well, the remote nature of this study site made a full scale post classification accuracy assessment impossible. One must caution, therefore, that the acceptability of the terrain model shown here is dependent upon the scale required.

Some preliminary attempts at using mathematical models to describe the L-band radar return from these same forest stands, for example, indicate that dense undergrowth in regenerating stands may dominate the return. Also, at pixel scale resolutions (25 m or less) the statistical separation on a pixel-by-pixel basis of flooded versus non-flooded stands becomes less certain (Wang *et al.*, 1989). Although these findings rely very heavily on extrapolated biometric data, which also contain error, it indicates that flood boundary delineation through moderately sized tree canopies using L-band radar will have accuracy limitations as a function of spatial resolution and statistical separability. This is not surprising for this formation where the SBL (with the exception of pneumatophores) is smooth. Many samples are required to differentiate between a truly flooded SBL and a merely wet one. The presence of pneumatophore fields can further complicate this situation.

CONCLUSIONS

Despite some uncertainties regarding canopy densities and complicating effects of incidence angle and SBL conditions, a reasonable digital topographic terrain model of a portion of the 12.5-metre tall partially closed Sundarbans forest was generated using multiple sets of L-band SAR data and ancillary tide elevation information. The dominance of the canopy-to-suface-to-canopy interaction in the radar backscatter of flooded forests was used to create sub-canopy inundation maps which, when

merged with tide surface data, provided the means for generating topographic models. The model shown here corroborates earlier geomorphology surveys and matches the topographic layout of bordering forests converted to rice agriculture. Ideally, the forest canopy conditions should be free of heavy undergrowth if using L-band HH SAR data and models could be improved by using multiple sets of data at a constant incidence angle over the total range of tide elevations. The optimal SAR incidence angle will depend upon the characteristics of the forest (especially stem density), and longer wavelengths such as P-band may be required to achieve a two-bounce return signal in heavier canopies as are found in the Amazon flood plain. Such models can be an invaluable tool for studying and mapping mangrove and other wooded wetland ecosystems. These data can be used by ecologists for studying the formative processes of these ecosystems as well as assigning values of productivity potential to various units within formations of this type.

ACKNOWLEDGMENTS

The authors would like to acknowledge the Government of the Peoples Republic of Bangladesh, especially Drs. Abdul Gafoor and M. A. H. Pramanik of the Bangladesh Space Research and Remote Sensing Organization, The Bangladesh Forest Department, and the Bangladesh Department of Hydrography. The authors would also like to thank the British Overseas Development Administration for their support.

REFERENCES

Chapman, V. J., 1975. *Mangrove Vegetation*. Cramer, Lehre.

Cimino, J. B., C. Elachi, and M. Settle, 1986. SIR-B - The Second Shuttle Imaging Radar Experiment. *IEEE Trans. Geo. Sci. and Remote Sensing*, Vol. GE-24, No. 4.

Daily, M., 1983. Hue-Saturation-Intensity Split-Spectrum Processing of Seasat Radar Imagery. *Photogrammetric Engineering & Remote Sensing* Vol. 49, No. 3, pp. 349–355.

Deb, S. C., 1956. Paleoclimatology and Geophysics of The Gangetic Delta. *Geographical Rev. India*, Vol. RF8, pp. 11–18.

Dobson, M. C., F. T. Ulaby, D. R. Brunfeldt, and D. N. Held, 1986. External Calibration of SIR-B Imagery with Area-Extended and Point Targets. *IEEE Trans. Geosci. & Remote Sens.*, Vol. GE-24, No. 4, pp. 453–461.

Engheta, N., and C. Elachi, 1982. Radar Scattering from a Diffuse Vegetation Layer over a Smooth Surface, *IEEE Transactions Geoscience and Remote Sensing*, Vol. GE-20, No. 2.

Golly, F., H. T. Odum, and R. F. Wilson, 1962. The Structure and Reproduction of a Puerto Rican Red Mangrove Forest in May. *Ecology*, Vol. 43, No. 1, pp. 9–19.

Hoffer, R., D. F. Lozano-Garcia, D. D. Gillespie, P. W. Mueller, and M. J. Ruzek, 1986. Analysis of Multiple Incidence Angle SIR-B Data for Determining Forest Stand Characteristics, *2nd Space Borne Imaging Radar Symposium*, JPL, Pasadena, California.

Imhoff, M., M. Story, C. Vermillion, F. Khan, and F. Polcyn, 1986. Forest Canopy Characterization and Vegetation Penetration Assessment With Space-Borne Radar. *IEEE Trans. Geosci. and Remote Sensing*, Vol. FSE-24, No. RF, pp. 535–542.

Krohn, M. D., N. M. Milton, and D. B. Segal, 1983. Seasat Synthetic Aperture Radar (SAR) Response to Lowland Vegetation Types in Eastern Maryland and Virginia. *Journal of Geophysical Research*, Vol. RF8, No. FS3, pp. 1937–1952.

Lugo, A. E., and S. C. Snedeker, 1974. The Ecology of Mangroves. *Ann. Rev. Ecol. Syst.*, Vol. 5, pp. 39–64.

MacDonald, H. C., W. P. Waite, and J. S. Demarke, 1980. Use of Seasat Satellite Radar Imagery for the Detection of Standing Water Beneath Forest Vegetation. *Technical Papers, ASP Annual Convention*, Niagra Falls, N.Y.

Ormsby, J. P., J. P. Blanchard, and A. J. Blanchard, 1985. Detection of Lowland Flooding Using Microwave Systems, *Photogrammetric Engineering & Remote Sensing*, Vol. 51, No. 3, pp 317–328.

Richards, J. A., G. Q. Sun, and D. S. Simonett, 1986. L-Band Radar Backscatter Modeling of Forest Stands. *IEEE Trans. Geosci. and Remote Sensing*, Vol. 25, pp. 487–498.

Shepherd, D., 1968. *A Two Dimensional Interpolation Function for Computer Mapping of Irregularly Spaced Data*. Paper #15, Geography and Properties of Surfaces Series, Laboratory for Computer Graphics and Spatial Analysis. Harvard University, Cambridge, Mass.

Treinish, L., 1989. An Interactive Discipline Independent Data Visualization System. *Computers and Physics Journal*, Vol. 3, Issue 3 (in press).

Ulbay, F. T., A. Tavakoli, C. Dobson, and T. B. A. Senior, 1986. Amplitude and Phase Propagation Constant of Vegetation. *IEEE International Geoscience and Remote Sensing Symposium, (IGARSS '86) Digest*, Zurich, Switzerland.

Waite, W. P., H. C. MacDonald, V. H. Kaupp, and J. S. Demarke, 1981. Wetland Mapping With Imaging Radar, *1981 International Geoscience and Remote Sensing Symposium*, Washington, D.C.

Waite, W. P., and H. C. MacDonald, 1971. Vegetation Penetration with K-band Imaging Radars, *IEEE Transactions on Geoscience and Electronics*, Vol. FSE-9, No. RF, pp. 147–155.

Wang, Y., M. Imhoff, and S. Simonett, 1989. Radar Modeling of Tropical Mangal Forest Studies. Paper in Preparation.

Zebker, H., J. VanZyl, and D. Held, 1987. Imaging Radar Polarimetry from Wave Synthesis, *Journal of Geophysical Research*, Vol. 92, No. B1, pp. 683–701.

(Received 10 March 1989; revised and accepted 7 February 1990)